RSC Advances

ROYAL SOCIETY OF CHEMISTRY

www.rsc.org/advances

Journal of Materials Chemistry B

ARTICLE

One-pot Synthesis of Fluorescent and Cross-linked Polyphosphazene Nanoparticles for Highly Sensitive and Selective Detection of Dopamine in Body Fluids

Daquan Wang,[a] Ying Hu,[b] Lingjie Meng,[a] Xiaochi Wang,[a] and Qinghua Lu[b]

Received 00th September 2015,
Accepted 00th September 2015

DOI: 10.1039/x0xx00000x

www.rsc.org/Materials B

Highly cross-linked and monodisperse polyphosphazene (PZS) nanoparticles exhibiting strong fluorescence were prepared by the facile one-pot polycondensation of hexachlorocyclotriphosphazene and 4′,5′-dibromofluorescein (DBF). Fluorescent DBF units were 'immobilized' and 'isolated' in the cross-linked structures to effectively overcome their concentration-quenching effect and improve their photobleaching properties. The resulting DBF–PZS nanoparticles emitted bright yellow fluorescence at any concentration and exhibited excellent resistance to photobleaching as well as interference from bio-molecules such as proteins, ascorbic acid and uric acid. Intriguingly, the fluorescence of the DBF–PZS nanoparticles was linearly quenched by DA range from 0.5 to 15 μg·mL^{-1} DA concentration via photoinduced charge transfer. Therefore, DBF–PZS nanoparticles represent a simple but effective, highly sensitive and selective detection method with a direct read out for DA in biological fluids.

1. Introduction

Dopamine (DA) is one of the most important catecholamine neurotransmitters in the mammalian central nervous system; it plays a key role in several brain functions and behavioural responses such as feeling, cognition and emotion.[1, 2] Typically, the excess secretion of DA often causes euphoria; sometimes, it even causes metabolic disturbances and untimely death.[3] In contrast, the lack of DA in the brain may lead to neurological disorders, such as schizophrenia and Parkinson's disease.[4, 5] Hence, it is imperative to monitor and quantify the concentration of DA in biological fluids such as urine and serum. However, the concentration of DA in living systems is quite low (ca. 4.9 – 7.6 μg·mL^{-1}) or even lower.[6, 7] In addition, the detection of DA is often subject to interference from other natural biological chemicals such as proteins and other catecholamine neurotransmitters, particularly, ascorbic acid (AA) and uric acid (UA)[8, 9]. Hence, developing a facile, extremely sensitive and selective analytical method for the detection of DA in actual body fluids remains a challenge.

Several methods have been developed for the quantification of DA, such as fluorescence spectroscopy[7,10,11], electrochemistry[12, 13], spectrophotometry[14, 15], capillary electrophoresis[16, 17], high-performance liquid chromatography[18] and surface acoustic wave method[19]. Among them, fluorescence methods have attracted significant attention, caused by their advantages such as high sensitivity, good reproducibility, ease operation and low cost. Organic dyes with tunable structure and optical properties appear to be the most versatile fluorescence probes. However, intrinsic limitations of conventional dyes such as the concentration-quenching effect[20] and poor photostability[21] have posed considerable difficulties for the further development of high-sensitivity detection techniques. Though it can improve the photobleaching of dyes by incorporating dye molecules inside a silica or polymer particle[22,23], organic dyes frequently tend to aggregate together and lead to fluorescence quenching or leak from the nanoparticles.[24] Tang et al developed an aggregation-induced emission (AIE) method that can overcome the concentration-quenching effect of the small fluorescent probes.[20, 25] The non-planar molecules might effectively overcome the aggregation-caused quenching by the restriction of the intramolecular rotation. Therefore, the fluorescence intensity of AIE probes is closely related to the aggregation state of probes. In practical applications, the fluorescence properties of probes are expected to be aggregation-independent to achieve high signal-to-noise ratio. In addition, an ideal fluorescence probe for highly sensitive and selective detection should also have strong fluorescence, high chemical and optical stability, good solvent dispersibility, excellent resistance to other external interference.

[a] School of Science; State Key Laboratory for Mechanical Behaviour of Materials,
Xi'an Jiaotong University, Xi'an 710049 (P. R. China)
Email: menglingjie@mail.xjtu.edu.cn
[b] School of Chemistry and Chemical Engineering,
Shanghai Jiaotong University, Shanghai 200240 (P. R. China)
Email: qhlu@sjtu.edu.cn

Electronic Supplementary Information (ESI) available: Fig. S1-S5. See DOI: 10.1039/x0xx00000x

2.Experiment Section

2.1 Chemicals and Reagents.

4',5'-dibromofluorescein (DBF, 95%), hexachlorocyclotriphosphazene (HCCP, 98%) and dopamine (DA, 98%) were purchased from Aladdin Reagent Corporation. Uric acid, ascorbic acid, acetic acid (HAc), sodium acetate trihydrate ($NaAc{\cdot}3H_2O$), triethylamine, were obtained from Shanghai Chemical Reagent Corporation. All other organic solvents, such as acetonitrile, acetone, anhydrous ethanol were of analytical grade, and were used as received. Water was purified using a Milli-Q-system (Millipore, Bedford).

2.2 Preparation of DBF–PZS Nanoparticles

In a typical experiment, DBF (32 mg, 65.3 μmol), TEA (2 mL) and acetonitrile (40 mL) were added into a 100 mL round-bottom flask. After ultrasonic irradiation for 20 min (50 W, 40 kHz), HCCP (15 mg, 43.1 μmol) in acetonitrile (10 mL) was added. The solution was maintained under ultrasonic irradiation for an additional 8 h. As soon as the reaction was completed, the resultant product was collected by centrifugation, successively washed with anhydrous alcohol (3 × 30 mL) and deionized water (3 × 30 mL), and dried at 45 °C under vacuum overnight.

2.3 Body Fluid Sample Collection and Pre-treatment

Two human serum samples and two human urine samples were collected from two healthy male volunteers (aged 24 years). All samples were subjected to a 50-fold dilution before analysis, and no other pre-treatments were necessary.

2.4 Measurement Procedures of DA in Body Fluid

A DBF–PZS aqueous suspension (3.0 $mg{\cdot}mL^{-1}$, 0.3 mL), a certain amount of DA (0.3 $mg{\cdot}mL^{-1}$) standard solution or body fluid sample and certain amounts of NaAc–HAc buffer (0.01 M, pH 5.0) were added into a 4 mL calibrated test tube. The total volume of mixture was 3 mL. The mixture was placed into a constant-temperature oscillator at 37 °C for 10 min. Then, the mixture was taken out from the oscillator and allowed to cool to room temperature for 5 min. Fluorescence measurements were conducted at an excitation wavelength of 470 nm and an emission wavelength of 558 nm.

2.5 Characterizations

Transmission electron microscopy (TEM) was performed on a CM120 (Philips). Field emission scanning electron microscope (FESEM) images were obtained using a Philips Sirion 200 instrument under an accelerating voltage of 20 kV. The size and distribution of all as-prepared nanomaterials were determined from TEM and SEM micrographs using ImageJ (V1.41, NIH, USA) for image analysis. Photographs were taken with a digital camera (IXUS 800IS, Canon, Japan). Fourier-transform infrared (FTIR) spectra were recorded on a Paragon 1000 (Perkin Elmer) spectrometer. Samples were dried overnight at 45 ºC under vacuum and thoroughly mixed and crushed with KBr to fabricate KBr pellets. X-ray photoelectron spectroscopy (XPS) experiments were carried out on a RBD upgraded PHI-5000C ESCA system (Perkin Elmer) with Mg Ka radiation (hv = 1253.6 eV) or Al Ka radiation (hv = 1486.6 eV). Ultraviolet and visible (UV-Vis) absorption spectra were carried out on a Shimadzu UV-2550 spectrophotometer. The fluorescence spectra were performed on a Perkin–Elmer LS 50B fluorescence spectrometer.

3. Results and discussion

To meet all the relevant criteria, we developed a new strategy to 'isolate' and 'fasten' fluorescent moieties into stable cross-linked polyphosphazene (PZS).[26, 27] The fluorescent moiety therefore exhibited high fluorescence efficiency at any concentration and exhibited improved resistance to photobleaching and other external interference. Here we show the first example of fluorescent and cross-linked PZS-containing 4′,5′-dibromofluorescein (DBF) to demonstrate the proof-of-concept of a highly sensitive and selective biosensor for the detection of DA. The fluorescence intensity of the as-prepared DBF–PZS nanoparticles at 558 nm was linearly quenched in DA solution concentration ranging from 0.5 to 15.0 $\mu g{\cdot}mL^{-1}$. The detection limit was calculated to be as low as 0.0018 $\mu g{\cdot}mL^{-1}$ (S/N = 3). The quenching effect should result from photoinduced charge transfer (PCT) between DA and DBF moieties. Amazingly, DBF–PZS nanoparticles exhibited high sensitivity and selectivity for the detection of DA over proteins and other neurotransmitters. Hence, we successfully used them for accurately measuring DA in actual urine and serum samples.

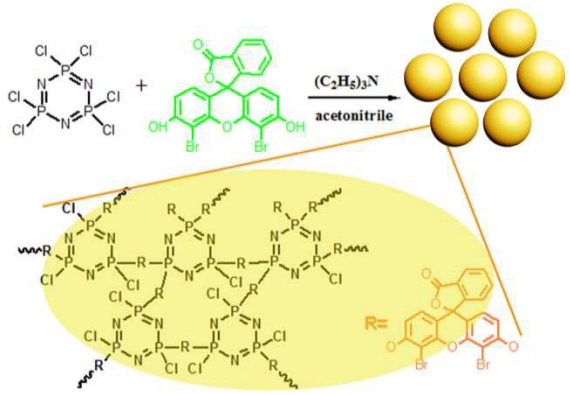

Scheme 1 Synthetic route to fluorescent DBF–PZS nanoparticles.

DBF–PZS nanoparticles are a type of cross-linked inorganic–organic hybrid polymer; they were prepared by a straightforward one-pot process according to Scheme 1. The polymerization of DBF and hexachlorocyclotriphosphazene (HCCP) in acetonitrile was performed in an ultrasonic bath with excess triethylamine (TEA), which could activate the phenolic hydroxyl groups of DBF to attack the nucleus of the phosphorus atoms of HCCP, thereby generating pre-polymer and HCl. TEA can also absorb the resulting HCl to speed up polymerization. As polymerization proceeded, the ultimately formed monodisperse DBF–PZS nanoparticles precipitated out of the solvent. The size and morphology of the synthesized DBF-PZS nanoparticles were investigated by field-emission scanning electron microscopy (FESEM) and transmission electron microscopy (TEM). As shown in Fig. 1a and b, the prepared DBF–PZS nanoparticles were monodisperse nanospheres, and their average diameter is approximately 354.0 ± 11.0 nm (Fig. 1d). As shown in Fig. 1c, the TEM image further proved that the nanoparticles are nanospheres having a diameter of 332.6 nm with a relatively smooth surface, which is in good agreement with results obtained from SEM images. Fourier transform infrared (FTIR) spectroscopy was employed to confirm the successful formation of DBF–PZS (see ESI, Fig. S1). Absorption peaks were observed at 626 and 530 cm^{-1}, which are attributed to the weakening of P–Cl

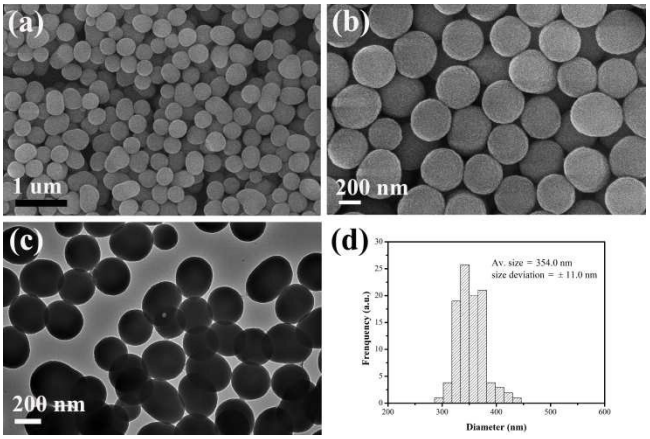

Fig. 1 (a, b) FESEM and (c) TEM images of DBF–PZS nanoparticles; (d) particle size distribution from (a).

in the DBF–PZS spectrum as compared to that of HCCP, while a new intense absorption peak was observed at 950 cm^{-1}, attributed to the P–O–Ph band; both provide direct evidence for the polymerization of HCCP and DBF[28, 29]. Other characteristic peaks of DBF–PZS were also be observed at 1184 cm^{-1} (P=N), 882 cm^{-1} (P–N) in the cyclotriphosphazene structure and at 1773 cm−1 (carboxylic ester), 1588 cm^{-1} and 1502 cm^{-1} (phenyl), 1105 cm^{-1} and 1050 cm^{-1} (C–O–C) in the DBF units. The presence of absorption peaks at 626 and 530 cm^{-1} in DBF–PZS suggests that the chlorine atoms are not completely replaced. X-ray photoelectron spectroscopy (XPS) analysis shows that the molar ratio between phosphorus (2p, 133.1 eV) and chloride (2p3, 198.0 eV) was approximately 1:1, suggesting that only one chlorine atom is replaced by DBF on each phosphorus atom owing to the steric hindrance effect (see ESI, Fig. S2).

The fluorescence emission spectra of DBF–PZS and DBF were measured to compare their fluorescence behavior (Fig. 2). The aqueous solution of DBF exhibited strong green fluorescence at 536 nm (inset of Fig. 2), but the aqueous suspension of DBF–PZS exhibits yellow emission at 558 nm, attributed to the enhanced planar conformation or the aggregation of DBF units in the DBF–PZS nanoparticles. Interestingly, DBF–PZS exhibited a remarkable

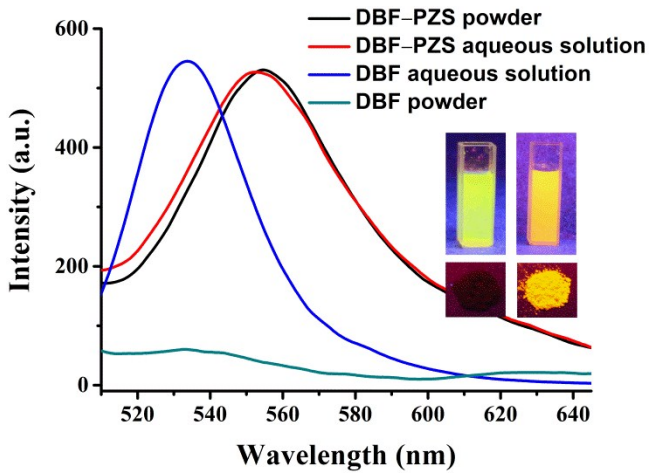

Fig. 2 Fluorescence spectra of DBF (470 nm excitated) and DBF–PZS (470nm excitated) in the suspension and solid states; inset shows the photos of corresponding DBF (left) and DBF–PZS (right) in the suspension (top) and solid states (bottom) under UV light (365 nm) illumination.

fluorescent emission feature in both the suspension and solid states, while DBF molecules almost lost all their fluorescence in the solid state, caused by aggregation-induced quenching. Notably, the cyclotriphosphazene rings are non-conjugated systems for electron transfer; they are also photochemically inert because their backbone consists of alternating P–N single and double bonds without any resonance[30, 31]. Therefore, the cyclotriphosphazene rings serve as spacers to isolate the DBF units after the DBF molecules are isolated and fixed in highly cross-linked structures. The transfer of electrons as well as energy among the DBF units was effectively blocked in the DBF–PZS nanoparticles, thereby decreasing fluorescence quenching at any DBF–PZS nanoparticles in both the solution and solid states was visualized from fluorescence images shown in the inset of Fig. 2. Amazingly, as compared to DBF, DBF–PZS nanoparticles exhibited superior resistance to photobleaching (see ESI, Fig. S3), indicating that the DBF moieties exhibit improved photochemical stability after being 'immobilized' in the cross-linked structures.

Fluorescein such as DBF represent a type of vital fluorescent probes that exhibit pH-dependent fluorescent property; in addition, it has been extensively used to measure intracellular pH[32, 33]. Hence, the fluorescent properties of DBF–PZS nanoparticles and DBF molecules at different pH were investigated by fluorescence spectroscopy (see ESI, Fig. S4 and S5). The DBF aqueous solution exhibited negligible fluorescence

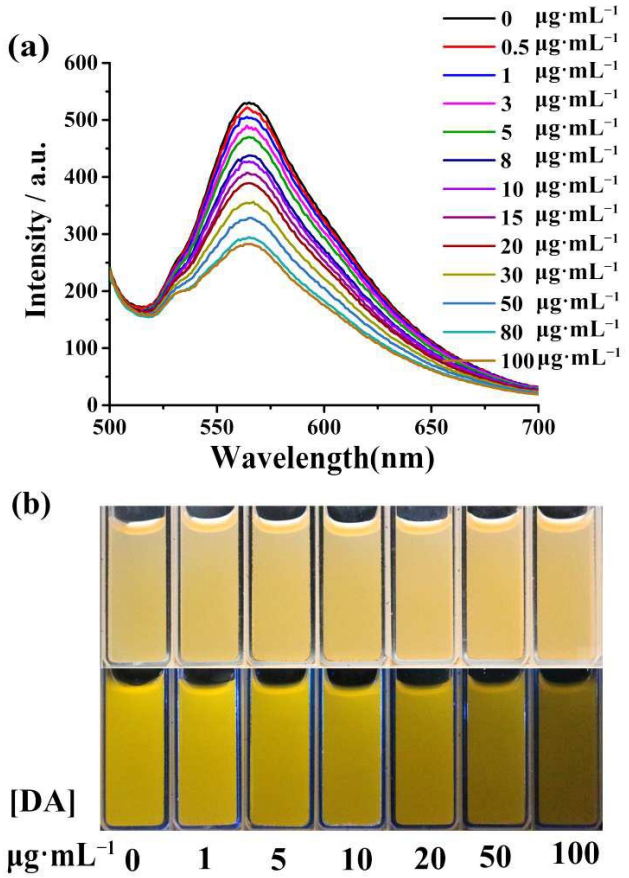

Fig. 3 (a) Fluorescence spectra (470nm excitated) and (b) the optical photograph (up) and fluorescence images (down) of DBF-PZS in NaAc-HAc buffer (0.3 $mg·mL^{-1}$) in the presence of different amounts of dopamine (0 – 100 $μg·mL^{-1}$).

at a lower than 5. However, the DBF aqueous solution gradually emitted stronger and stronger green fluorescence with the increase in pH from 5 to 12, indicating obvious pH-dependent fluorescent properties (see ESI, Fig. S4). The aqueous suspension of DBF–PZS also exhibited pH-dependent emission. It exhibited a very weak emission at a low pH (< 5) and exhibited strong fluorescence with greater than 20 nm red-shift at higher pH (see ESI, Fig. S5).

An appropriate pH has to be chosen for accurately measuring DA by a fluorescence method. Notably, although the fluorescence intensity of DBF–PZS significantly enhanced with increasing pH, a series of complex chemical oxidative polymerization reactions rapidly occurred in DA molecules under basic and natural pH conditions, which in turn can stagnate the experiment[34, 35]. The acidic environment is beneficial for the stability of DA, but it leads to an inferior fluorescence intensity of DBF–PZS. Fortunately, DBF–PZS still exhibited a relatively strong fluorescence at pH 5.0. Taking the above mentioned results into account, a NaAc–HAc buffer solution (0.01 M, pH 5.0) instead of body fluid pH (approximately 7.4) was recommended here to obtain the fluorescence spectra of DBF–PZS with the presence of different amounts of DA (0–100 μg·mL^{-1}).

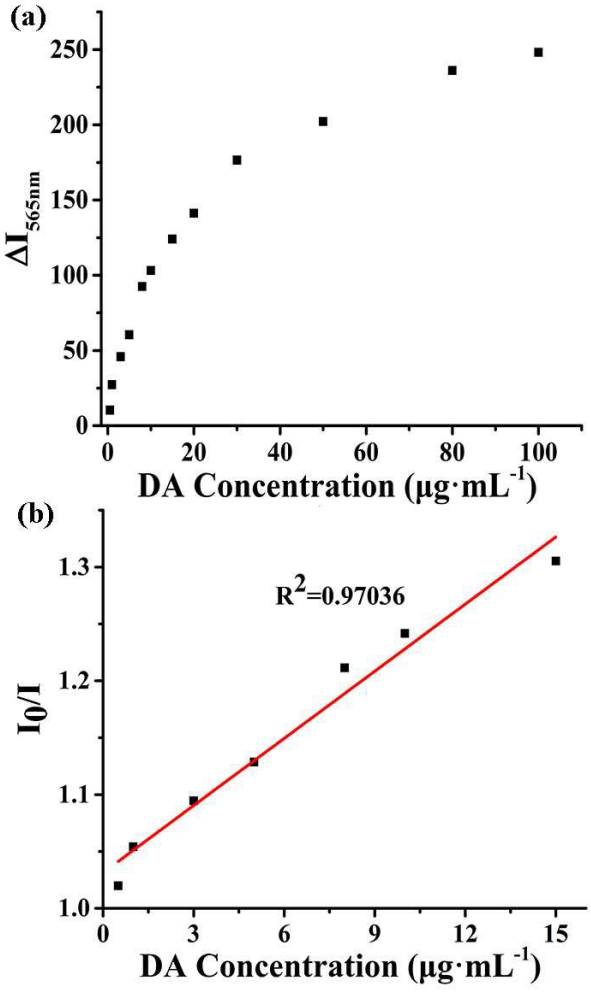

Fig. 4 (a) Plot of the quenched fluorescence intensity at 558 nm based on Fig. 3a, (ΔI) versus DA concentration ([DA]); (b) plot of I_0/I against [DA].

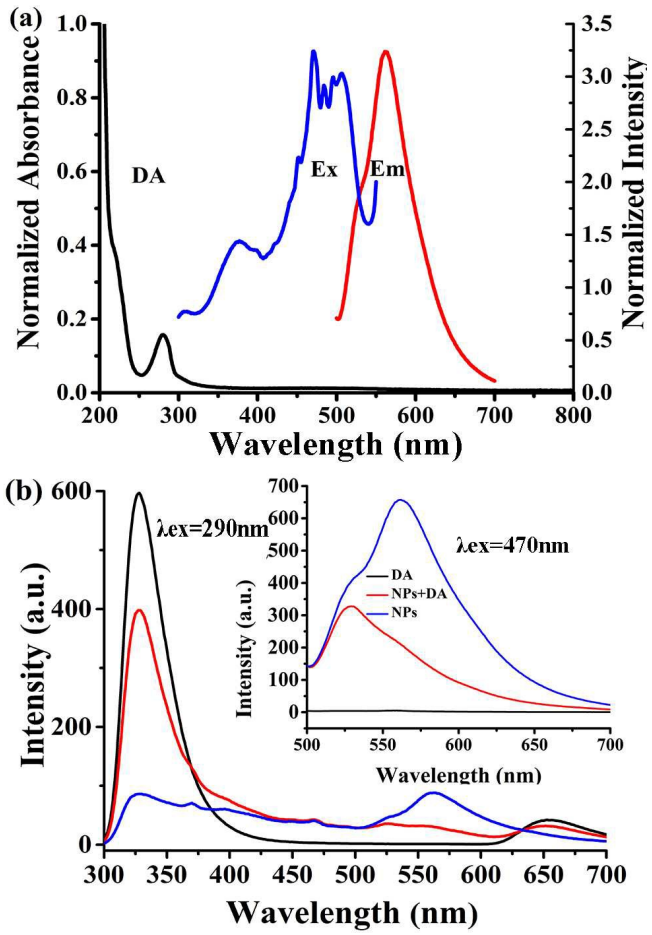

Fig. 5 (a) UV–Vis absorption spectra of DA (black), fluorescence excitation and emission spectra of DBF-PZS (blue and red, respectively); (b) steady–state fluorescence spectra of 30 μg·mL^{-1} DA (black), the mixture of DBF-PZS NPs and DA (red), and 300μg·mL^{-1} DBF-PZS (blue) in NaAc-HAc solution (0.01M, pH 5.0) under excitation of 290 nm in a high pass of 300 nm filter (inset: under excitation of 470 nm).

The fluorescence quenching of DBF–PZS nanoparticles in a pH 5.0 NaAc–HAc buffer solution using different concentrations of DA was investigated (Fig. 3). The fluorescent property of DBF–PZS nanoparticles is very sensitive to the presence of DA. With the increase in the concentration of DA (0.5 – 100 μg·mL^{-1}) added, the emission intensity of the DBF–PZS suspension gradually decreased (Fig. 3a). The fluorescence changes can be also observed from the fluorescence images (Fig. 3b).

The difference of the fluorescence intensity (ΔI) of DBF–PZS at 558 nm was closely related to the DA concentration ([DA]). The increase of ΔI was roughly characterized by linearity at low DA concentrations, i.e. 0.5 – 15 μg·mL^{-1}; however, it gradually deviated from the linear relationship at higher DA concentration (Fig. 4a). The fluorescence quenching of DBF–PZS by DA can be also quantitatively described as a typical Stern–Volmer-type equation:

$$\frac{I_0}{I} = 1 + K_{SV}[DA] \qquad (1)$$

Here, I_0 and I represent the fluorescence intensities of DBF–PZS in the absence and presence of DA, respectively, and KSV is the Stern–Volmer quenching constant; it can be calculated by the

slope of the equation (1). As shown in Fig. 4b, the plot of I_0/I at 558 nm against [DA] exhibited linearity from 0.5 to 15 μg·mL^{-1} with a KSV value of 19.67 L·g^{-1}.

The fluorescence quenching of the excited-state DBF–PZS nanoparticles is attributed to either PCT or fluorescence resonance energy transfer (FRET). DA exhibited a strong absorption peak at around 280 nm, while DBF–PZS exhibited an emission peak at approximately 558 nm (Fig. 5a). There was no overlap region observed between the absorption peak of DA and the emission peak of DBF–PZS, implying that the fluorescence quenching mechanism of DBF–PZS by DA is independent of FRET. The emission intensities of both DBF–PZS at 558 nm and DA at 325 nm simultaneously decreased, indicating that fluorescence quenching is attributed to electronic interaction on the attachment of DA to DBF–PZS nanoparticles (Fig. 5b).36 The DA molecules are hypothesized to exhibit a tendency to attach onto DBF moieties by π–π stacking and hydrogen bonding, and an efficient and rapid electron and energy transfer from the excited DBF moieties to DA can readily occur. Hence, the DBF–PZS nanoparticles represent a novel label-free PCT biosensor for the detection of DA. Typically, the fluorescence of organic dyes is quenched in complex biological environments, caused by their interaction with biomolecules[37-39]. Although the fluorescence intensity of DBF markedly decreased after mixing with a bovine serum albumin (BSA) solution, the fluorescence intensity of DBF–PZS was stable with negligible fluorescence quenching (Fig. 6). Most of the DBF moieties were speculated to be immobilized in the nanoparticles and could not interact with BSA. In addition, the fluorescence of DBF–PZS was not significant changed in the presence of AA (100 μg·mL^{-1}) and UA (100 μg·mL^{-1}), which are components mainly present in blood (Fig. 6). The above results suggest that the developed DBF–PZS fluorescent biosensor renders highly favorable and specific fluorescence recognition of DA. The improved resistance of DBF–PZS nanoparticles to the interference from biomolecules benefits their applications for the detection of DA in actual body fluid samples. Hence, these novel fluorescent PZS-based biosensors were used for the detection of DA in low-dilution biological fluids (50- fold dilution of urine and serum). Although the body fluids excited at 470 nm exhibited a fluorescence background at 558 nm, this fluorescence background did not affect the quantitative recovery

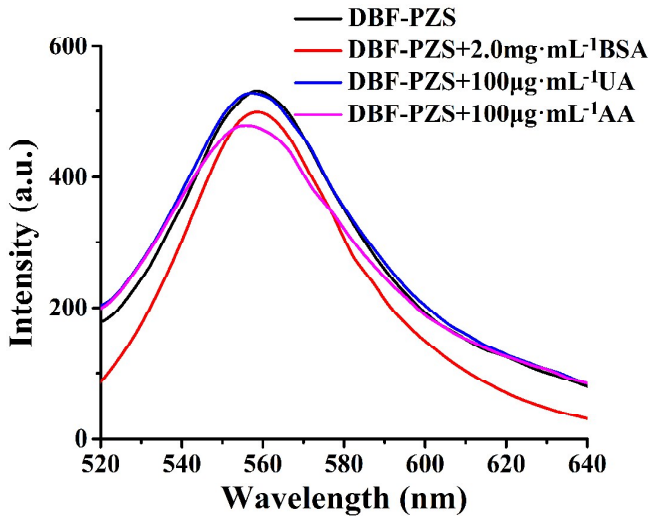

Fig. 6 Fluorescence spectra (470nm excitated) of DBF-PZS (300 μg·mL^{-1}) in the presence of UA (100 μg·mL^{-1}) and AA (100 μg·mL^{-1}), BSA (2.0 mg·mL^{-1}), respectively.

Samples	DA concentration (μg·mL^{-1}) spiked	measured (mean ± std dev, n = 3)	recovery % (mean ± std dev, n = 3)
human serum-1	1.0	1.1 ± 0.1	110.0 ± 10.0
	3.0	2.9 ± 0.2	97.0 ± 7.0
	5.0	5.2 ± 0.1	104.0 ± 2.0
human serum-2	1.0	1.0 ± 0.1	100.0 ± 4.0
	3.0	2.8 ± 0.2	93.0 ± 7.0
	10.0	9.8 ± 0.3	98.0 ± 3.0
human urine-1	1.0	1.0 ± 0.1	100.0 ± 10.0
	3.0	2.8 ± 0.2	93.0 ± 7.0
	5.0	5.2 ± 0.1	104.0 ± 2.0
human urine-2	1.0	1.1 ± 0.1	110.0 ± 10.0
	3.0	2.9 ± 0.2	97.0 ± 7.0
	10.0	9.9 ± 0.2	99.0 ± 2.0

Table 1 Results for the Detection of Dopamine in Human Urine and Serum Samples

(93%–110%) of spiked DA (Table 1). To the best of our knowledge, these results represent the few reported examples for the use of fluorescent nanoparticles as a highly selective and sensitive biosensor for the accurate quantification of DA in actual body fluids.

In summary, highly cross-linked and monodisperse DBF–PZS nanoparticles with an average diameter of 354.0 ± 11.0 nm were prepared by facile one-pot polycondensation. The DBF–PZS nanoparticles exhibited remarkable fluorescence emission properties in the suspension and solid states because isolated DBF units were fastened in the cross-linked structures. The fluorescence of the DBF–PZS nanoparticles was linearly quenched by DA in DA concentration ranging from 0.5 to 15 μg·mL^{-1}. The detection limit of DBF–PZS by DA is as low as 0.0018 μg·mL^{-1}, indicating high sensitivity for DA detection. In addition, other biomolecules such as proteins and other neurotransmitters such as UA and AA did not interfere with DA detection. Hence, this study demonstrates a simple but effective, highly sensitive and selective detection method with a direct readout for DA.

4. Conclusions

In summary, highly cross-linked and monodisperse DBF–PZS nanoparticles with an average diameter of 354.0 ± 11.0 nm were prepared by facile one-pot polycondensation. The DBF–PZS nanoparticles exhibited remarkable fluorescence emission properties in the suspension and solid states because isolated DBF units were fastened in the cross-linked structures. The fluorescence of the DBF–PZS nanoparticles was linearly quenched by DA in DA concentration ranging from 0.5 to 15 μg·mL^{-1}. The detection limit of DBF–PZS by DA is as low as 0.0018 μg·mL^{-1}, indicating high sensitivity for DA detection. In

addition, other biomolecules such as proteins and other neurotransmitters such as UA and AA did not interfere with DA detection. Hence, this study demonstrates a simple but effective, highly sensitive and selective detection method with a direct readout for DA.

Acknowledgement

This work was supported by National Natural Science Foundation of China (21174087, 21474079), the Major Project of Chinese National Programs for Fundamental Research and Development (973 Project: 2009CB930400), the Program for New Century Excellent Talents in University (NCET-13-0453), the China Postdoctoral Science Foundation (2013M540738, 2014T70909), the Fundamental Funds for the Central Universities (08143101).

Notes and references

1 Kriks, S.; Shim, J.-W.; Piao, J.; Ganat, Y. M.; Wakeman, D. R.; Xie, Z.; Carrillo-Reid, L.; Auyeung, G.; Antonacci, C.; Buch, A.;Yang, L.; Beal, M. F.; Surmeier, D. J.; Kordower, J. H.; Tabar,V.; Studer, L. *Nature* 2011, **480**, 547-U177.

2 Chien, E. Y. T.; Liu, W.; Zhao, Q.; Katritch, V.; Han, G. W.; Hanson, M. A.; Shi, L.; Newman, A. H.; Javitch, J. A.; Cherezov, V.; Stevens, R. C. *Science* 2010, **330**, 1091-1095.

3 Mittal, S. K.; Eddy, C. *Behav. Neurol.* 2013, **26**, 255-263.

4 Michel, P. P.; Toulorge, D.; Guerreiro, S.; Hirsch, E. C. *FASEB J.* 2013, **27**, 3414-3423.

5 Howes, O. D.; Kambeitz, J.; Kim, E.; Stahl, D.; Slifstein, M.; Abi- Dargham, A.; Kapur, S. *Arch. Gen. Psychiatry* 2012, **69**, 776-786.

6 She, G.; Huang, X.; Jin, L.; Qi, X.; Mu, L.; Shi, W. *Small* 2014, **10**, 4685-4692.

7 Zhang, X.; Chen, X.; Kai, S.; Wang, H.-Y.; Yang, J.; Wu, F.-G.; Chen, Z. *Anal. Chem.* 2015, **87**, 3360-3365.

8 Noroozifar, M.; Khorasani-Motlagh, M.; Taheri, A. *Talanta* 2010, **80**, 1657-1664.

9 Zhang, Y. Z.; Cai, Y. J.; Su, S. *Anal. Biochem.* 2006, **350**, 285-291.

10 Qu, K.; Wang, J.; Ren, J.; Qu, X., *Chem. Eur. J.* 2013, **19**, 7243-7249.

11 Lin, Y.; Yin, M.; Pu, F.; Ren, J.; Qu, X. *Small* 2011, **7**, 1557-1561.

12 Farjami, E.; Campos, R.; Nielsen, J. S.; Gothelf, K. V.; Kjems, J.; Ferapontova, E. E. *Anal. Chem.* 2013, **85**, 121-128.

13 Sun, C.-L.; Chang, C.-T.; Lee, H.-H.; Zhou, J.; Wang, J.; Sham, T.-K.; Pong, W.-F. *Acs Nano* 2011, **5**, 7788-7795.

14 Feng, J.-J.; Guo, H.; Li, Y.-F.; Wang, Y.-H.; Chen, W.-Y.; Wang, A.-J. *ACS Appl. Mater. Interfaces* 2013, **5**, 1226-31.

15 Biao, K.; Anwei, Z.; Yongping, L.; Yang, T.; Yanyan, Y.; Guoyue, S. *Angew. Chem. Int. Ed.* 2011, **50**, 1837-40.

16 Zhao, Y.; Zhao, S.; Huang, J.; Ye, F. *Talanta* 2011, **85**, 2650-2654.

17 Bouri, M.; Lerma-García, M. J.; Salghi, R.; Zougagh, M.; Ríos, A. *Talanta* 2012, **99**, 897-903.

18 Syslová, K.; Rambousek, L.; Kuzma, M.; Najmanová, V.; Bubeníková-Valešová, V.; Šlamberová, R.; Kačer, P. *J. Chromatogr. A* 2011, **1218**, 3382-3391.

19 Fourati, N.; Seydou, M.; Zerrouki, C.; Singh, A.; Samanta, S.; Maurel, F.; Aswav, D. K.; Chehimi, M. *ACS Appl. Mater. Interfaces* 2014, **6**, 22378-22386.

20 Hong, Y.; Lam, J. W. Y.; Tang, B. Z., *Chem. Soc. Rev.* 2011, **40**, 5361-5388.

21 Eggeling, C.; Widengren, J.; Brand, L.; Schaffer, J.; Felekyan, S.; Seidel, C. A. M. *J. Phys. Chem. A* 2006, **110**, 2979-2995.

22 Montalti, M.; Prodi, L.; Rampazzo, E.; Zaccheroni, N. *Chem. Soc. Rev.* 2014, **43**, 4243-4268.

23 Xu-dong, W.; Meier, R. J.; Wolfbeis, O. S. *Adv. Funct. Mater.* 2012, **22**, 4202-4207.

24 Zhao, X. J.; Bagwe, R. P.; Tan, W. H. *Adv. Mater.* 2004, **16**, 173-176.

25 Luo, J. D.; Xie, Z. L.; Lam, J. W. Y.; Cheng, L.; Chen, H. Y.; Qiu, C. F.; Kwok, H. S.; Zhan, X. W.; Liu, Y. Q.; Zhu, D. B.; Tang, B. Z., *Chem. Commun.* 2001, 1740-1741.

26 Hu, Y.; Meng, L.; Lu, Q. *Langmuir* 2014, **30**, 4458-4464.

27 Meng, L.; Xu, C.; Liu, T.; Li, H.; Lu, Q.; Long, J. *Polym. Chem.* 2015, **6**, 3155-3163.

28 Hu, Y.; Meng, L.; Niu, L.; Lu, Q. *Langmuir* 2013, **29**, 9156-9163.

29 Zhou, J.; Meng, L.; Lu, Q. *J. Mater. Chem.* 2010, **20**, 5493-5498.

30 Breza, M. *Polyhedron* 2000, **19**, 389-397.

31 Potin, P.; Dejaeger, R. *Eur. Polym. J.* 1991, **27**, 341-348.

32 Yin, W.; Zhu, H.; Wang, R. *Dyes Pigments* 2014, **107**, 127-132.

33 Kurabayashi, T.; Funaki, N.; Fukuda, T.; Akiyama, S.; Suzuki, M. *Anal. Sci.* 2014, **30**, 545-550.

34 Ju, K.-Y.; Lee, Y.; Lee, S.; Park, S. B.; Lee, J.-K. *Biomacromolecules* 2011, **12**, 625-632.

35 Lee, H.; Dellatore, S. M.; Miller, W. M.; Messersmith, P. B. *Science* 2007, **318**, 426-430.

36 Sykora, M.; Petruska, M. A.; Alstrum-Acevedo, J.; Bezel, I.; Meyer, T. J.; Klimov, V. I. *J. Am. Chem. Soc.* 2006, **128**, 9984-9985.

37 Saunders, M. J.; Block, E.; Sorkin, A.; Waggoner, A. S.; Bruchez, M. P. *Bioconj. Chem.* 2014, **25**, 1556-1564.

38 Ji, Z.; Liang, X.; Sun, Y.; Fan, J. *Asian J. Chem.* 2014, **26**, 521-526.

39 Abou-Zied, O. K.; Sulaiman, S. A. J. *Dyes Pigments* 2014, **110**, 89-96.